RSC Advances

PAPER

Cite this: *RSC Adv.*, 2024, **14**, 24838

One-dimensional magnetic chains for methylene blue removal

Cheng Luo and Yan Li*

Adsorption is a promising method for the treatment of wastewater from the dyestuff industry due to its simplicity, high efficiency, low energy consumption and no secondary pollution. The capacity to separate adsorbents in a timely and efficient manner is a crucial factor in industrial applications. One-dimensional magnetic chains modified with polydopamine and *in situ* generated Ag nanoparticles (MC@PDA–Ag) were fabricated as highly regenerable adsorbents for methylene blue (MB). The magnetic chains were characterized by scanning electron microscopy, thermogravimetric analysis, Fourier transform infrared spectroscopy, nitrogen adsorption/desorption, X-ray photoelectron spectrometry, X-ray diffraction and magnetometry. The adsorption and catalytic degradation of MB by the materials were investigated. The regeneration capacity of MC@PDA–Ag was also evaluated. The specific saturation magnetization of MC@PDA–Ag is 38.2 emu g^{-1}. The adsorption capacity of MC@PDA–Ag remained 76% of the initial value after 12 cycles of adsorption and elution. The novel adsorbents, which integrate adsorption and catalytic degradation, are anticipated to facilitate the development of magnetic adsorption materials for the remediation of dye pollution.

Received 6th June 2024
Accepted 1st August 2024

DOI: 10.1039/d4ra04142a

rsc.li/rsc-advances

1. Introduction

Synthetic dyes are employed in a multitude of industrial sectors, including textiles, paper, leather manufacturing, food processing, plastics, cosmetics and printing. Unfortunately, a substantial amount of wastewater containing dyes is produced during the manufacturing and utilization of dye products, which represent the primary source of environmental pollution.[1] Although the cytotoxicity, genotoxicity and carcinogenicity risks associated with various synthetic dyes vary considerably, such exposure has been demonstrated to have adverse effects on human health.[2] It is therefore highly important for public health to adopt an efficient, environmentally friendly and cost-effective treatment method for dye-containing wastewater.

A multitude of chemical, biological and physical approaches have been proposed for the removal of dyes from wastewater.[2] Adsorption is a promising approach for the removal of dyes from wastewater and has advantages in terms of its ease of operation, high efficiency and low energy consumption.[3,4] In recent years, polydopamine (PDA) has emerged as a biomimetic material inspired by the mussel adhesion protein. It can be readily deposited on a diverse range of materials.[5] A significant number of catechol and heterocyclic nitrogen atoms in PDA can combine with other substances through electrostatic interactions, coordination or chelation, hydrogen bonding, π–π stacking, and other functions. These interactions facilitate the efficient adsorption of contaminants.[6] Furthermore, the reductive properties of the catechol groups enable the reduction of Ag ions to Ag nanoparticles. Ag nanoparticles can act as catalysts for the reduction of organic substances in the presence of sodium borohydride ($NaBH_4$) as an electron donor.[7]

In addition to adsorption capacity of the adsorbent, its recovery performance is of critical importance for its industrial application. The capacity of magnetic materials to migrate in a specific direction in response to an external magnetic field can be harnessed to create magnetic adsorbents, which can be employed for the magnetic separation of adsorbents. However, the separation of magnetic nanoparticles from aqueous solutions requires a robust magnetic field. Assembling magnetic nanoparticles into magnetic microspheres has the potential to reduce the magnetic field strength needed, thereby improving the separation efficiency. We employed a polymerization-induced colloidal aggregation method to prepare magnetic urea–formaldehyde microspheres.[8] Following silica modification, the urea–formaldehyde resin was removed at high temperature, resulting in the preparation of magnetic microspheres with high specific saturation magnetization (61.38 emu g^{-1}). The microspheres can be rapidly separated under a magnetic field.

Assembling magnetic particles into larger structures can further improve the magnetic separation efficiency and reduce separation time. In the presence of magnetic field, magnetic particles spontaneously arrange into one-dimensional chain structure due to magnetic dipole–dipole interactions.[9] The one-dimensional chain structure can be stabilized by coating the surface of the chain structure with an organic or inorganic

School of Medicine, Yichun University, Yichun, 336000, People's Republic of China. E-mail: liyan@jxycu.edu.cn

shell.[10,11] Nevertheless, magnetic microsphere chains with high specific saturation magnetization for the remediation of wastewater containing dyes have rarely been studied.

Herein, we applied a magnetic field during the preparation of magnetic urea–formaldehyde microspheres. This resulted in the spontaneous assembly of the microspheres into a one-dimensional magnetic chain with urea–formaldehyde resin (MCUF). Following silica modification, the urea–formaldehyde resin will be removed at high temperature to obtain magnetic chains (MC) with high specific saturation magnetization. Then, the synthesis of PDA-modified MC (PDA@MC) was achieved through the oxidative self-polymerization of dopamine hydrochloride in an alkaline environment. The reductive properties of the PDA shell facilitated the formation of Ag nanoparticles on the surface of the magnetic carrier, thereby yielding MC@PDA–Ag composites. Adsorption and degradation of MB and recycling of the MC@PDA–Ag composites were achieved utilizing the high adsorption performance of the PDA shell and the catalytic performance of the Ag nanoparticles (Fig. 1). The specific saturation magnetization of MC@PDA–Ag is 38.2 emu g^{-1}, which is a high value among micron-sized magnetic adsorbents. The chain structure, comprising multiple magnetic microspheres, enables rapid separation under a magnetic field due to the collective magnetic field force exerted by the microspheres. MC@PDA–Ag was found to exhibit dye adsorption, separation and catalytic degradation properties. Furthermore, the adsorption capacity of MC@PDA–Ag remained 76% of the initial value after 12 cycles of adsorption and elution. This study has developed a novel adsorbent with high adsorption capacity, rapid separation and recycling capabilities, which will promote the industrial applications of magnetic materials in the field of organic pollutant treatment.

2. Experimental

2.1 Materials

Tris and urea were purchased from Sangon Biotech (Shanghai, China). Dopamine hydrochloride, tetraethyl orthosilicate (TEOS), silver nitrate, MB, rhodamine B (Rh B), malachite green (MG), methyl orange (MG), sodium borohydride and Fe_3O_4 nanoparticles (20 nm) were obtained from Aladdin Chemistry (Shanghai, China). Ethanol, formaldehyde (37–40%), ammonia (25–28%), hydrochloric acid (36–38%), nitric acid (65–68%) and sodium hydroxide were purchased from Sinopharm Chemical Reagent Co. (Shanghai, China). All reagents were of analytical grade and used without further purification. Deionized water was used in all experiments.

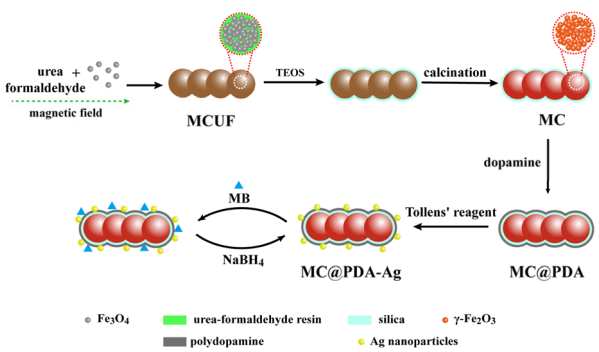

Fig. 1 Schematic diagram of the preparation of one-dimensional magnetic chains modified with dopamine and *in situ* generated Ag nanoparticles, which are employed as highly renewable adsorbents for the removal of MB.

2.2 Preparation of magnetic chains with urea–formaldehyde resin (MCUF)

A suspension containing 12 g of Fe_3O_4 nanoparticles, 1.28 mL of concentrated nitric acid and 400 mL of deionized water was sonicated for 3 h at 70 °C with stirring. A homogeneous colloidal solution (water-based ferrofluids) was obtained after centrifugation at a speed of 3000 rpm for 10 min. 0.32 mL of concentrated nitric acid, 8 mL of urea solution (0.25 g mL^{-1}) and 4 mL of formaldehyde solution (37%) was added to 100 mL of water-based ferrofluids. The mixture was mixed evenly by stirring and placed in a magnetic field at room temperature. Magnetic microspheres with aggregated Fe_3O_4 nanoparticles and urea–formaldehyde resin were subsequently formed and lined according to the magnetic field, which led to the formation of magnetic chains. The magnetic chains with urea–formaldehyde resin (MCUF) were separated with a magnet and washed with deionized water.

2.3 Preparation of magnetic chains (MC)

0.1 g of MCUF was dispersed in 10 mL of deionized water. Subsequently, 40 mL of anhydrous ethanol, 1 mL of ammonia, and 0.05 mL of tetraethyl orthosilicate were added. The reaction proceeded for 5 h under stirring. The silica-modified magnetic chains were separated and placed in a constant-temperature blast drying oven at 60 °C for drying. The urea–formaldehyde resin was removed by programmed temperature-raising calcination (50–500 °C, 2 °C min^{-1}). MC with high specific saturation magnetization was obtained.

2.4 Preparation of polydopamine-modified MC (MC@PDA)

0.4 g of MC was dispersed in a mixed solution of 45 mL of Tris buffer (20 mM) and 45 mL of anhydrous ethanol. Subsequently, 0.2 g of dopamine hydrochloride in 10 mL of 50% ethanol was added to above reaction mixture. The reaction proceeded for a specified period of time (5, 10, 24 h) under stirring to encapsulate MC with a PDA shell (MC@PDA).

2.5 Preparation of MC@PDA–Ag composites

0.1 g of MC@PDA was added to 40 mL of Tollens' reagent (10 mg mL^{-1}) and stirred for 12 h. This process allowed the generation of Ag nanoparticles *in situ via* the reductive capacity of the PDA shell, thus forming MC@PDA–Ag composites. Subsequently, the composites were washed with water and ethanol before being subjected to drying in a constant-temperature blast dryer.

2.6 Characterization

The morphologies of MC@PDA and MC@PDA–Ag composites were observed by scanning electron microscopy (SEM) with Phenom G2 Pro desktop scanning electron microscope (New York, USA). The chemical compositions of the composites were characterized by energy dispersive spectrometer. Fourier transform infrared spectra (FTIR) of the samples were recorded with Bruker Optics Tensor 27 spectrometer (Ettlingen, Germany). Thermogravimetric analysis (TGA) was performed using Mettler Toledo TGA/DSC 1 thermogravimetric analyzer (Zurich, Switzerland) in air from 50 °C to 800 °C with a temperature ramp of 10 °C min^{-1}. The crystallinity of the MC@PDA–Ag composites was characterized by powder X-ray diffraction (XRD) on Shimadzu XRD-7000 X-ray diffractometer (Tokyo, Japan). The magnetic properties were tested on Lake Shore 7410 vibrating-sample magnetometer (Maryland, USA) at room temperature. The textural parameters of MC and MC–PDA were determined *via* nitrogen adsorption/desorption using Micromeritics ASAP2460 adsorption analyzer (Atlanta, USA). The specific surface area of the samples was determined using the Brunauer–Emmett–Teller (BET) method. The surface elemental composition and chemical binding information was characterized by Thermo Fisher Scientific K-Alpha X-ray photoelectron spectrometer (XPS) (Boston, USA). The C 1s peak at 284.8 eV was used as a binding energy reference for handling the surface charging effects.

2.7 Adsorption experiments

The effects of adsorption time, pH and concentrations of MB on adsorption capacity were invested. For adsorption time, 50 mg of MC@PDA was added to 16 mL of MB solution (pH 10, 100 mg L^{-1}) and stirred for 20, 40, 60, 80, 100 and 120 min. For pH, 50 mg of MC@PDA was added to 16 mL of MB solution (100 mg L^{-1}) with different pH and stirred for 2 h. For concentrations of MB, 50 mg of MC@PDA was added to 16 mL of MB solution (pH 10) with different concentrations (10, 25, 50, 75, 100, 150, 200 mg L^{-1}) and stirred for 2 h. After the magnetic composites were separated by a magnet, the changes in MB concentration were investigated by UV absorption spectroscopy.

To evaluate the adsorption performance for different dyes, MC@PDA–Ag was added separately to MB, Rh B, MG and MO solutions (pH 10, 100 mg L^{-1}) and stirred for 2 h. After the magnetic composites were separated by a magnet, the changes in dye concentration were investigated by UV absorption spectroscopy.

2.8 Catalytic degradation experiments

To clarify the catalytic degradation of MB by MC@PDA–Ag, 20 mg of MC@PDA or MC@PDA–Ag was added to 10 mL of MB solution (10 mg mL^{-1}). Subsequently, 0.5 mL of $NaBH_4$ solution (0.1 mol L^{-1}) was added. After the magnetic composites were separated by a magnet, the changes in MB concentration in the solution were recorded.

The stability of MC@PDA–Ag in aqueous solutions with different pH (2, 3, 7, 10, 11) was investigated. After dispersed in solutions with different pH for 24 h, 20 mg of MC@PDA–Ag was added to 10 mL of MB solution (40 mg mL^{-1}). Subsequently, 0.5 mL of $NaBH_4$ solution (0.1 mol L^{-1}) was added. The magnetic composites were separated after 3 min by a magnet. The changes of MB concentration in the solution were recorded.

2.9 Recycling of the MC@PDA–Ag composites

MC@PDA or MC@PDA–Ag composites with adsorbed MB were firstly washed with 2 mL of $NaBH_4$ solution (1.5 mmol L^{-1}). Subsequently, the composites were further washed with ethanol for 2 times. The composites were reused for MB adsorption to assess their regeneration and recycling capacities.

3. Results and discussion

3.1 Adsorbent characteristics

The newly generated magnetic urea–formaldehyde resin microspheres were oriented and arranged into a one-dimensional chain structure during the synthesis in a magnetic field. Subsequently, the urea–formaldehyde resin and Fe_3O_4 nanoparticles proceeded to aggregate on the surface of the chain structure, resulting in the formation of MCUF. Following silica modification, the internal urea–formaldehyde resin of MCUF is eliminated by calcination under atmospheric conditions, resulting in the formation of MC (Fig. 2a).

Furthermore, MC was encapsulated with a PDA shell to obtain MC@PDA by dispersing MC in an alkaline solution of dopamine for a period of time. In comparison to the yellowish-brown color of the MC dispersion, the MC@PDA dispersion appears black-brown (Fig. 2b). As shown in the FTIR spectra (Fig. 2c), the characteristic Fe–O peak (635 cm^{-1}) appears in all three microspheres.[12] The characteristic absorption peaks of urea–formaldehyde resin (*e.g.*, the C=O and C–N stretching

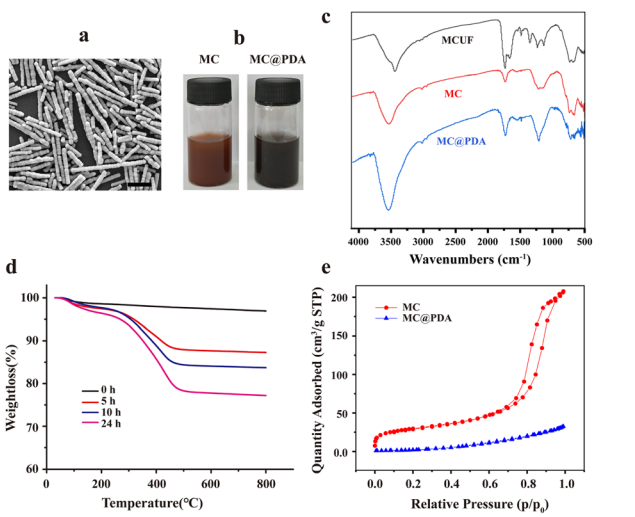

Fig. 2 (a) SEM image of MC (scale: 10 μm). (b) Digital images of MC and MC@PDA dispersion. (c) FTIR spectra of MCUF, MC and MC@PDA. (d) Thermogravimetric analysis of MC–PDA with different dopamine self-polymerization time. (e) Nitrogen adsorption/desorption isotherms of MC and MC@PDA.

vibration peaks at 1640 cm^{-1} and 1560 cm^{-1}, respectively) were less intense in MC than in MCUF, indicating that high temperature effectively removed the urea–formaldehyde resin.[8] The presence of Si–O stretching (1120 cm^{-1}) and Si–O bending (945 cm^{-1})[13] indicated that silica modification had occurred in MC and MC@PDA. Following the modification of PDA onto the silica surface,[14–16] the absorption peaks of MC@PDA at 3440 cm^{-1}, 1640 cm^{-1}, and 1110 cm^{-1} exhibited a notable increase.

As the self-polymerization time of dopamine prolongs, the deposition of PDA on the surface of MC will increase. Thermogravimetric analysis revealed that the weight loss during heating process gradually increased with prolonged self-polymerization time (Fig. 2d), reflecting increasing specific gravity of PDA in MC@PDA.

Fig. 2e shows the nitrogen adsorption–desorption isotherms for MC and MC@PDA, revealing significant variations in their textural parameters. The MC@PDA exhibits a BET surface area of 12.5 $m^2 g^{-1}$ and a total pore volume of 0.0502 $cm^3 g^{-1}$, which are both smaller than those of MC (104.1 $m^2 g^{-1}$ and 0.3244 $cm^3 g^{-1}$). The pore size of MC was 147.85 Å, while the pore size of MC@PDA decreased to 54.65 Å. The pore structure of MC is filled with PDA during modification, resulting in decreases in specific surface area, pore volume and pore size. Although the specific surface area of MC@PDA decreased after PDA modification, it is still high enough to endow MC@PDA with large amounts of binding sites for dye adsorption.

The reducing property of PDA enabled the reduction of Ag ions and the generation of Ag nanoparticles on the surface of MC@PDA, thus producing MC@PDA–Ag.[17] After high temperature calcination, the urea–formaldehyde resin was removed. The presence of Ag nanoparticles and PDA coating on the surface of the MC@PDA–Ag particles were confirmed through XPS analysis. The XPS survey spectrum of MC@PDA–Ag (Fig. 3a) reveals the presence of Ag, C, N and O. Fe and Si, distributed inside the material and coated by PDA shell, was hard to detect due to limited penetration depth. In the high-resolution XPS spectrum of Ag 3d (Fig. 3b), two peaks at ~368.02 and ~374.02 eV could be ascribed to Ag $3d_{5/2}$ and Ag $3d_{3/2}$ respectively, demonstrating the existence of Ag nanoparticles. The C 1s spectrum (Fig. 3c) can be assigned to C–C (284.79 eV), C–N (285.58 eV), C–H (284.08 eV), C–O–C (286.38 eV) and O–C=C (288.54 eV), respectively. The N 1s spectrum (Fig. 3d) can be assigned to $-NH_2$ (401.03 eV), –N–H (399.61 eV) and –N= (398.28 eV), respectively. The XPS analysis demonstrated the successful deposition of PDA coating and formation of Ag nanoparticle.

XRD analysis was conducted to characterize the crystal structure of MC@PDA–Ag. In addition to the γ-Fe_2O_3 crystalline phase (transformed by oxidation of Fe_3O_4 nanoparticles at elevated temperatures), distinct Ag diffraction peaks were observed in XRD pattern of MC@PDA–Ag (Fig. 4a). The particle size of the Ag nanoparticles was 20.9 nm calculated using Scherrer's formula. To provide a more visual characterization of the presence of Ag nanoparticles on the surface of MC@PDA–Ag, we analyzed the particles using SEM and EDS. The results indicated that only minimal background signals were observed for the elemental analysis of Ag on MC@PDA, whereas pronounced Ag signals were evident for MC@PDA–Ag, confirming the presence of Ag (Fig. 4b). The magnetic properties of the samples were quantified by means of a vibrating sample magnetometer. MC, MC@PDA, and MC@PDA–Ag exhibited specific saturation magnetization values of 56.9 emu g^{-1}, 43.4 emu g^{-1}, and 38.2 emu g^{-1}, respectively (Fig. 4c). The chain-like structures, comprising multiple magnetic microspheres, are subjected to considerably stronger magnetic field forces than a single magnetic microsphere. This property enables these structures to separate rapidly in a magnetic field.

3.2 Adsorption potential for MB

MB is a synthetic dye with significant health hazards and has been used in a variety of industrial sectors including textiles and paper. The discharge of wastewater containing MB without

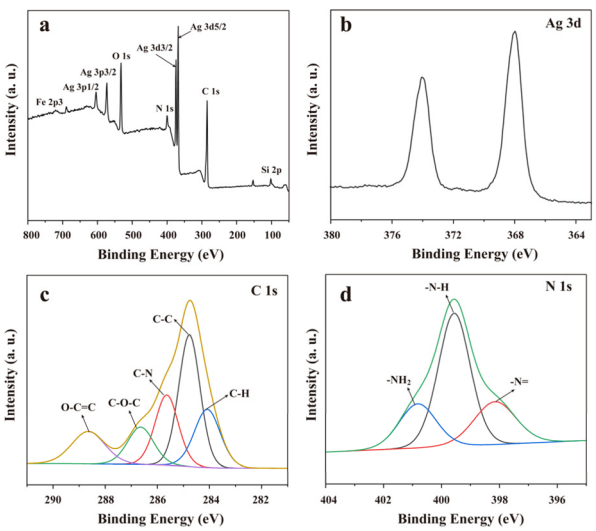

Fig. 3 Survey scan XPS spectrum (a), high-resolution XPS spectra of Ag 3d (b), C 1s (c), and N 1s (d) regions of MC@PDA–Ag.

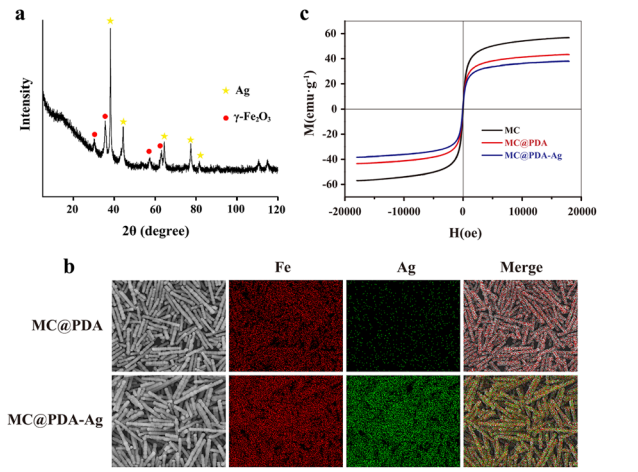

Fig. 4 (a) XRD pattern of MC@PDA–Ag. (b) SEM/EDS analysis of MC@PDA and MC@PDA–Ag. (c) Magnetization curve of MC, MC@PDA and MC@PDA–Ag.

effective treatment can result in significant water pollution and contribute to a reduction in the availability of clean water resources.[18] The potential of MC@PDA for water purification was evaluated through the removal of MB. PDA can bind with MB through electrostatic interactions and π–π interactions, resulting in rapid adsorption of MB by PDA.[19] As shown in Fig. 5a, following 10 h of oxidative polymerization of dopamine on the MC surface, the MB adsorption capacity of MC@PDA reached 75% within 1 min and nearly 90% within 20 min. It is evident that the adsorption capacity of MC@PDA for MB exhibits a pronounced increase during the initial phase, followed by a gradual acceleration until the equilibrium state is reached after 40 min. Despite the PDA shell of MC@PDA became thicker as the PDA modification time increased, the adsorption capacity of MC@PDA did not exhibit a similar trend: the maximum adsorption capacity for MB was 38.2 mg g^{-1} when the PDA modification time was 10 h. Upon prolonging the modification time to 24 h, a pronounced reduction in the adsorption capacity was observed. These findings suggest that the adsorption of MB mainly occurs on the surface of the PDA shell. Consequently, the modification time of the PDA was set at 10 h, while the adsorption time was fixed at 2 h in all subsequent experiments.

MB is a positively charged molecule, whereas the PDA shell exhibits different charge states as pH changes, with an isoelectric point of approximately 4. Consequently, the difference in pH influences the electrostatic adsorption between the two materials. Specifically, the PDA surface becomes deprotonated as the pH of the solution increases (Fig. 5b), promoting electrostatic attraction between the positively charged MB molecules and the negatively charged PDA. The adsorption capacity of MC@PDA for MB gradually increased as the pH increasing within the range of 2–10 (Fig. 5c). This finding is consistent with previous studies of PDA microspheres.[19] The MB adsorption capacity of MC@PDA increased with increasing initial MB concentration. At an initial concentration of 200 mg L^{-1}, the adsorption capacity reached 48.7 mg g^{-1} (Fig. 5d).

The dye adsorption capacity of MC@PDA–Ag towards MB, MG, Rh B, and MO was also investigated. As shown in Fig. 5e, the adsorption capacities are 36.64, 38.06, 7.12, and 2.92 mg g^{-1}, respectively. Due to the negative charge of PDA at pH 10, MC@PDA–Ag shows higher adsorption capacity for cationic dyes (MB, MG and Rh B) and lower adsorption capacity for anionic dye (MO). MC@PDA–Ag could effectively adsorb MB from mixtures of MB and MO (Fig. 5f).

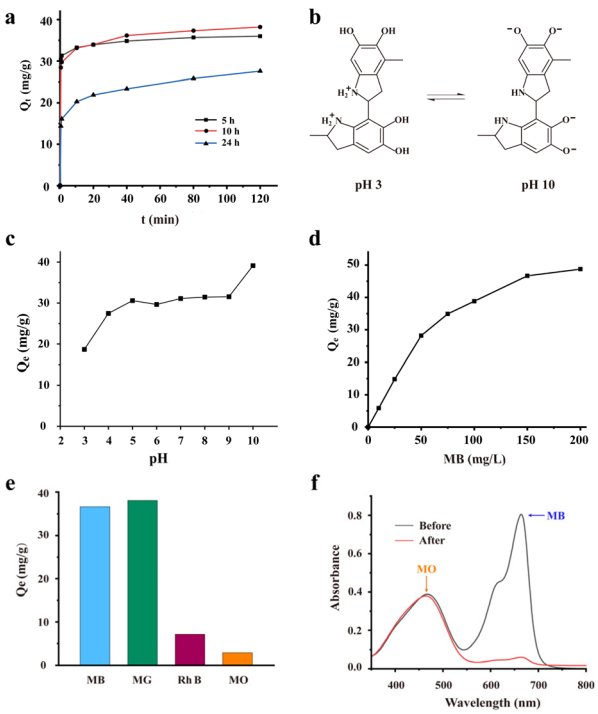

Fig. 5 Dye removal capacity of MC@PDA and MC@PDA–Ag. (a) The impact of dopamine self-polymerization time on adsorption capacity of MC@PDA. (b) Structure of PDA at pH 3 and 10. The impact of pH (c) and initial concentration of MB (d) on the adsorption capacity of MC@PDA. (e) The adsorption capacities of MC@PDA–Ag for different dyes. (f) The ultraviolet-visible spectra of mixtures of MB (5 mg L^{-1}) and MO (5 mg L^{-1}) before and after adsorption by MC@PDA–Ag.

3.3 Catalytic degradation of MC@PDA–Ag

Ag nanoparticles exhibit excellent catalytic properties,[20] enabling the reduction of MB by $NaBH_4$ into colorless leucomethylene blue (LMB) (Fig. 6a) The efficiency of MC@PDA–Ag in catalysing the reduction of MB by $NaBH_4$ was evaluated in comparison to that of MC@PDA (Fig. 6b). As the duration of the experiment increased, MB was gradually adsorbed by MC@PDA, resulting in a concomitant decrease in the absorbance curve of the solution. The adsorption rate decreased as the adsorption time increased. After 10 min, approximately 40% of the MB remained in solution (Fig. 6b, left). This was due to the superficial active sites on the PDA shell of MC@PDA gradually became saturated, making the subsequent adsorption increasingly difficult. The combination of the adsorption

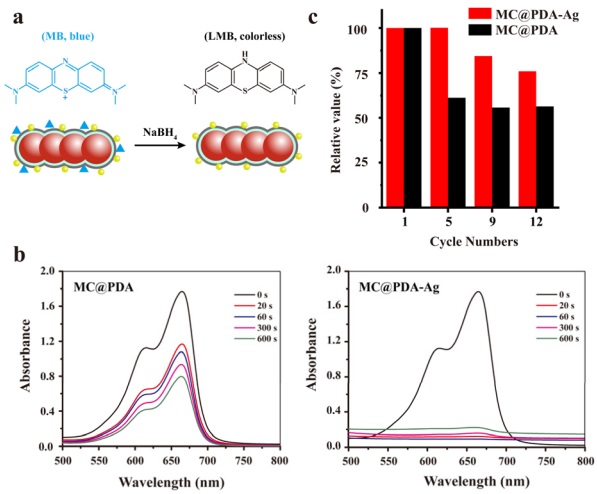

Fig. 6 (a) The catalytic degradation of MB by MC@PDA–Ag. (b) The ultraviolet-visible spectra of MB following its removal by MC@PDA (left) and MC@PDA–Ag (right). (c) Reusability of MC@PDA and MC@PDA–Ag.

capacity of PDA and the catalytic reduction capability of Ag nanoparticles results in the rapid scavenging of MB by MC@PDA–Ag. This is evidenced by the complete disappearance of the characteristic peaks of MB within 20 s (Fig. 6b, right). Once the MB was catalytically reduced to LMB, it will leave the active sites of the PDA shell for decreased electrostatic adsorption. The PDA shell can continue to adsorb MB in solution. This process was repeated until the MB in solution was completely removed.

3.4 Reusability of MC@PDA–Ag

To circumvent the potential for secondary pollution resulting from the direct addition of $NaBH_4$ to wastewater, a two-step process was employed to remove MB. Initially, MB was adsorbed onto MC@PDA–Ag. After magnetically separated and concentrated, $NaBH_4$ was added allowing MB catalytically degraded by Ag nanoparticles. The elution and regeneration of the adsorbent are achieved at the same time. The adsorption capacity of MC@PDA–Ag remained 76% of its initial value even after 12 adsorption–elution cycles (Fig. 6c). Nevertheless, the adsorption capacity of MC@PDA reduced to approximately 50% of its original value after 5 adsorption–elution cycles. This suggests that the catalytic degradation capacity of Ag nanoparticles facilitates a more efficient elution of MB. Therefore, the utilization of MC@PDA–Ag for the remediation of water pollution not only results in the catalytic degradation of MB, but also offers the advantage of multiple recycling capacities.

3.5 Stability of MC@PDA–Ag

PDA has high chemical stability under acidic conditions[21] and can effectively protect the internal Fe_3O_4 cores from etching.[22] The stability of MC@PDA–Ag in solutions with different pH (2, 3, 7, 10, and 11) was tested. After 24 h of storage, the catalytic degradation performance of MC@PDA–Ag towards MB (40 mg mL^{-1}) was evaluated. The remaining MB concentrations after 3 min were almost the same for pH 3, 7, 10 and 11 (Table 1), proving the stability of MC@PDA–Ag. Interestingly, when dispersed in solution of pH 2, MC@PDA–Ag quickly aggregated. However, after storage for 24 h, the catalytic performance of MC@PDA–Ag become stronger. The reason is currently unclear. It is probably due to the faster absorption of MB and the enhanced catalytic performance of Ag nanoparticles after aggregation.

Table 1 Catalytic activities of MC@PDA–Ag dispersed in solutions of different pH

pH	MB concentration after degradation (mg L^{-1})
2	0.22
3	1.65
7	1.84
10	1.30
11	1.54

4. Conclusions

One-dimensional magnetic chains were fabricated and modified with PDA, followed by *in situ* generation of Ag nanoparticles. MC@PDA–Ag exhibited high specific saturation magnetization, which enabled rapid magnetic separation of materials. The MC@PDA–Ag could be used for adsorption and catalytic degradation of dyes, and can be reused multiple times, rendering it an optimal candidate for use in the field of dye pollution treatment.

Data availability

The authors declare that the data supporting the results of this study are available in the paper.

Author contributions

C. Luo: implementation, data analysis, draft writing and revision; Y. Li: conceptualization, funding acquisition, supervision.

Conflicts of interest

There are no conflicts to declare.

Acknowledgements

This work was supported by the National Natural Science Foundation of China (No. 51763024), Natural Science Foundation of Jiangxi (No. 20202BAB214027), and the Science and Technology Research Project of Jiangxi Provincial Department of Education (GJJ2201736).

Notes and references

1 U. Ewuzie, O. D. Saliu, K. Dulta, S. Ogunniyi, A. O. Bajeh, K. O. Iwuozor and J. O. Ighalo, *J. Water Process Eng.*, 2022, **50**, 103273.
2 J. Lin, W. Ye, M. Xie, D. H. Seo, J. Luo, Y. Wan and B. Van der Bruggen, *Nat. Rev. Earth Environ.*, 2023, **4**, 785–803.
3 D. Lan, H. Zhu, J. Zhang, S. Li, Q. Chen, C. Wang, T. Wu and M. Xu, *Chemosphere*, 2022, **293**, 133464.
4 A. Ejsmont, S. Dutta, A. Jankowska, S. Wuttke and J. Goscianska, *Chem. Mater.*, 2024, **36**, 4468–4480.
5 H. Hemmatpour, O. De Luca, D. Crestani, M. C. A. Stuart, A. Lasorsa, P. C. A. van der Wel, K. Loos, T. Giousis, V. Haddadi-Asl and P. Rudolf, *Nat. Commun.*, 2023, **14**, 664.
6 F. Liu, R. Jamal, T. Abdiryim and X. Liu, *Cellulose*, 2022, **29**, 8025–8064.
7 K. Wang, X. Zhu, Y. Yang, D. Ye, R. Chen and Q. Liao, *J. Environ. Chem. Eng.*, 2022, **10**, 108253.
8 Y. Li, Y. Wu, C. Luo, F. Yang, L. Qin, T. Fu, G. Wei, X. Kang and D. Wu, *J. Mater. Chem. B*, 2013, **1**, 4644–4654.
9 Y. Chen and A. El-Ghazaly, *Small*, 2023, **19**, 2205079.
10 B. Kang, M.-K. Shin, S. Han, I. Oh, E. Kim, J. Park, H. Y. Son, T. Kang, J. Jung, Y.-M. Huh, S. Haam and E.-K. Lim, *BioChip J.*, 2022, **16**, 280–290.

11 X. Huang, M. Liu, Q. Lu, K. Lv, L. Wang, S. Yin, M. Yuan, Q. Li, X. Li, T. Zhao and D. Zhao, *Advanced Science*, 2024, 2309564.
12 J. Lin, X. Weng, R. Dharmarajan and Z. Chen, *Chemosphere*, 2017, **169**, 413–417.
13 M. E. Simonsen, C. Sønderby, Z. Li and E. G. Søgaard, *J. Mater. Sci.*, 2009, **44**, 2079–2088.
14 S. Chen, S. Chen, J. Lan, H. Qin, S. Yang, P. Wang and Y. You, *J. Alloys Compd.*, 2024, **977**, 173336.
15 S. Lu, B. Liang, J. Hu, Y. Liu, F. Yang and J. Liu, *Chem. Eng. J.*, 2024, **482**, 148990.
16 H. Wang, X. Guo, Y. Liu, M. Yi, L. Wan, S. Liao, Z. Wang and L. Fang, *Compos. Commun.*, 2022, **29**, 101049.
17 D. Wang, L. Bao, H. Li, X. Guo, W. Liu, X. Wang, X. Hou and B. He, *Nanoscale*, 2022, **14**, 6212–6219.
18 P. O. Oladoye, T. O. Ajiboye, E. O. Omotola and O. J. Oyewola, *Results Eng.*, 2022, **16**, 100678.
19 J. Fu, Z. Chen, M. Wang, S. Liu, J. Zhang, J. Zhang, R. Han and Q. Xu, *Chem. Eng. J.*, 2015, **259**, 53–61.
20 J. Saha, A. Begum, A. Mukherjee and S. Kumar, *Sustainable Environ. Res.*, 2017, **27**, 245–250.
21 T. Ataei-Germi and A. Nematollahzadeh, *J. Colloid Interface Sci.*, 2016, **470**, 172–182.
22 Y. Xie, B. Yan, H. Xu, J. Chen, Q. Liu, Y. Deng and H. Zeng, *ACS Appl. Mater. Interfaces*, 2014, **6**, 8845–8852.